JOURNAL OF SOLID STATE CHEMISTRY 120, 238–243 (1995)

Structure and Magnetic Properties of 6-Layered Hexagonal Oxides $Ba_3Cr_2MO_9$ (M = Mo and W)

Masahiro Shikano,[1] Osamu Ishiyama, Yoshiyuki Inaguma, Tetsurō Nakamura,[2] and Mitsuru Itoh[3]

Research Laboratory of Engineering Materials, Tokyo Institute of Technology, 4259 Nagatsuta, Midori-ku, Yokohama 227, Japan

Received October 11, 1994; revised May 19, 1995; accepted July 6, 1995

Structural analysis and measurement of magnetic susceptibility were carried out for the 6*H*-type hexagonal compounds $Ba_3Cr_2MO_9$ (M = Mo and W). The space groups of $Ba_3Cr_2MoO_9$ and $Ba_3Cr_2WO_9$ were determined by Rietveld analysis of powder X-ray diffraction data to be $P6_3/mmc$ and $P\bar{6}2c$, respectively. Chromium ions were found to occupy the centers of face-shared octahedra, with tungsten or molybdenum ions at the centers of corner-shared octahedra. The magnetic susceptibilities of $Ba_3Cr_2MoO_9$ and $Ba_3Cr_2WO_9$ were explained using the two-sublattice and dimer models, respectively; the difference may be due to the difference in the valence states of Cr and Mo in $Ba_3Cr_2MoO_9$ and Cr and W in $Ba_3Cr_2WO_9$. © 1995 Academic Press, Inc.

INTRODUCTION

A complex compound ABX_3 adopts a perovskite-type structure when the ratio of ionic radii involving A, B and X ions satisfies an appropriate geometric relation. Usually this is explained by a tolerance factor, t, defined by the geometric relation (1)

$$t \equiv \frac{r_A + r_X}{\sqrt{2}(r_B + r_X)}. \qquad [1]$$

Here, r_A, r_B, and r_X are the ionic radii of the A cation, the B cation, and the X anion, respectively. In the case $t \approx 1$, the crystal system of a compound tends to be cubic. When t is smaller, the crystal structure becomes distorted like the orthorhombic $GdFeO_3$-type (2). Some ABX_3 compounds exhibit hexagonal symmetry when $t > 1$. Hexagonal ABX_3 is classified by the stacking sequence of BX_6 octahedra (1), e.g., 2-layered $CsNiCl_3$ (2H) (1), 4-layered $BaMnO_3$ (4H) (3), 6-layered $BaTiO_3$ (6H) (4), and 9-layered $BaRuO_3$ (9H) (5). Other hexagonal compounds are known: 3-layered $Ba(Zn_{1/3}Nb_{2/3})O_3$ (6), 5-layered $Ba_5Ta_4O_{15}$ (7), 8-layered $BaLi_{1/4}Ta_{3/4}O_3$ (8), 10-layered $Ba_{10}W_6Li_4O_{30}$ (9), 12-layered $Ba_4Re_2Co_2O_{12}$ (10), and 24-layered $Ba_4Re_2Ba_2O_{12}$ (10).

In 6H compounds, there are two kinds of B sites, in the centers of corner-shared octahedra (B_1 site) and in face-shared octahedra (B_2 site). In $MNiF_3$ (M = Rb,Tl) (11), with the 6H structure, all the B sites are occupied by Ni^{2+} ions. These compounds are totally ferrimagnetic due to both the ferromagnetic 90° superexchange interaction between Ni^{2+} ions in the face-shared B_2 site and the antiferromagnetic 180° superexchange interaction of ions in the corner-shared B_1 site. In contrast, the magnetism of 6H-type $Ba_3Ru_2MO_9$ (M = Mg, Ca, Sr, and Cd) is explained by the isolated Ru–Ru dimer (12, 13) in the Ru_2O_9 cluster since pentavalent ruthenium ions and M ions occupy the face-shared B_2 site and corner-shared B_1 site (14, 15), respectively. It is to be noted that all the $Ba_3Ru_2MO_9$ compounds have the 6H structure, although the tolerance factor is in the range from 1.06 for $Ba_3Ru_2MgO_9$ to 0.98 for $Ba_3Ru_2SrO_9$.

The two compounds $Ba_3Cr_2MoO_9$ and $Ba_3Cr_2WO_9$ are also classified as 6H types, although Sr_2CrMoO_6 and Sr_2CrWO_6 have the perovskite-type structure (16). Sr_2CrMoO_6 and Sr_2CrWO_6 are ferrimagnetic as a result of B-site ordering (16). In the case of $Ba_3Cr_2MoO_9$ and $Ba_3Cr_2WO_9$, however, the details of magnetism and crystal structure are not clear. Since chromium, molybdenum, and tungsten are transition metals and belong to the same 6A group in the periodic table, the magnetic interaction among B-site cations is considered to be different from that in $Ba_3Ru_2MO_9$ (M = Mg, Ca, Sr, and Cd). In this paper, the structure and the relation between the magnetism and the valency state of the B-site cations of $Ba_3Cr_2MO_9$ (M = Mo and W) are discussed.

EXPERIMENTAL

The samples were synthesized by a conventional solid state reaction technique. Barium nitrate, dichromium tri-

[1] Present address: Osaka National Research Institute, AIST, MITI, 1-8-31 Midorigaoka, Ikeda, Osaka 563, Japan.

[2] Present address: Department of Applied Chemistry, Utsunomiya University, 2753 Ishii-cho, Utsunomiya, Tochigi 321, Japan.

[3] To whom correspondence should be addressed.

0022-4596/95 $12.00

oxide, tungsten trioxide, and molybdenum trioxide of 99.9% purity(Rare Metallic Co., Ltd.) were used as starting materials. The powders were thoroughly mixed in an agate mortar with ethanol and calcined for 10 hr at 1273 K on an alumina boat covered with platinum foil in a flow of nitrogen gas. The calcined powder was pulverized, pressed into pellets 10 mm in diameter and 2 mm in thickness at a pressure of 80 MPa, and sintered at 1243 K for 10 hr on an alumina boat in a flow of 97% argon and 3% hydrogen. Then the pellets were vacuum sealed in a quartz glass tube. This was heated at 1243 K for 10 hr and quenched to room temperature. Finally, the pellets were pulverized, washed with 0.1 mole $\cdot$ dm^{-3} hydrochloric acid using an ultrasonic cleaner to remove impurities such as $BaMoO_4$ and $BaWO_4$, and dried overnight *in vacuo* (16). After this treatment, $Ba_3Cr_2MoO_9$ was found to contain no impurity phase, but a small amount of $BaWO_4$ was recognized in $Ba_3Cr_2WO_9$. The identification of the prepared samples was carried out by powder X-ray diffraction with Cu$K\alpha$ radiation at room temperature using a MAC Science MXP^{18} diffractometer. The crystal structure of the samples was analyzed using the Rietveld analysis program, RIETAN (17). The data were collected with Cu$K\alpha$ radiation by accumulating counts for 1 sec at 0.02° intervals in the range $2\theta = 20°$–$100°$. The magnetic susceptibility of the samples was measured by a Quantum Design SQUID magnetometer (type MPMS 2) in the range 5–300 K and a Shimadzu Faraday-type magnetic balance (type MB-2) in the range 300–700 K. The core magnetism of the relevant ions were subtracted from the measured susceptibility. Measurement of the X-ray photoelectron spectrum was carried out using a Shimadzu ESCA-850. The Au $4f_{7/2}$ spectrum was used as a standard to calibrate the binding energy of the obtained spectra.

RESULTS AND DISCUSSION

Observed and refined X-ray powder diffraction profiles of $Ba_3Cr_2MoO_9$ and $Ba_3Cr_2WO_9$ are shown in Fig. 1. Results of the Rietveld analysis are summarized in Tables 1 and 2. During the refinement for $Ba_3Cr_2WO_9$ a two phase mixture of $Ba_3Cr_2WO_9$ and $BaWO_4$ was assumed and the peaks for $BaWO_4$ were excluded from Fig. 1. The space group of $Ba_3Cr_2MoO_9$ is assigned to $P6_3/mmc$ (No. 194), and its lattice parameters are a = 0.56938(2) nm and c = 1.3945(2) nm; the space group of $Ba_3Cr_2WO_9$ is assigned to $P\bar{6}2c$ (No. 190), and its lattice parameters are a = 0.56963(5) nm and c = 1.3985(1) nm. Although the space group of $Ba_3Cr_2MoO_9$ also could be assigned to $P\bar{6}2c$ or $P6_3/m$ (No. 176), the refinement using $P6_3/mmc$ showed the minimum value of the R factor. The results indicate that B-site cations are completely ordered; i.e., molybdenum (or tungsten) and chromium ions occupy the B_1 and the B_2 sites, respectively. Schematic representations of the ionic configuration are shown in Fig. 2, indicating that the environments of the B-site cations are almost similar even though the space groups are different from each other. Ionic radii of Cr^{3+}, Cr^{4+}, and O^{2-} are 0.0615, 0.055, and 0.140 nm (18), respectively, so that calculated interatomic distances are $d(Cr^{3+}$–$O^{2-}) = 0.202$ nm and $d(Cr^{4+}$–$O^{2-}) = 0.195$ nm. In Table 3, observed interatomic distances between chromium and $O(1)$ for $Ba_3Cr_2MoO_9$ and $Ba_3Cr_2WO_9$ are d(Cr–O(1)) = 0.200(3) and 0.201(3) nm, respectively. On the other hand, the interatomic distances between chromium and O(2) for other oxygens are d(Cr–O(2)) = 0.208(3) and 0.208(3) nm, respectively. These inconsistencies mean that the evaluation of the ionic distances using the ionic radii may not be effective in distorted structures such as hexagonal compounds containing face-shared octahedra. The interatomic distances between two chromium ions, d(Cr–Cr), in $Ba_3Cr_2MoO_9$ and $Ba_3Cr_2WO_9$ are 0.251 and 0.247 nm, respectively, and these values are comparable to those for Ba_2CrTaO_6 (19). The interatomic distances between W^{6+} or W^{5+} and O^{2-} and Mo^{6+} or Mo^{5+} and O^{2-} calculated using the ionic radii (18) are $d(W^{6+}$–$O^{2-}) = 0.200$ nm, $d(W^{5+}$–$O^{2-}) = 0.202$ nm, $d(Mo^{6+}$–$O^{2-}) = 0.199$ nm, and $d(Mo^{5+}$–$O^{2-}) = 0.201$ nm and they are fairly large compared to the observed value in Table 3. The stabilization of the hexagonal structure and the interionic distances for Ba_2CrTaO_6 have been discussed from the viewpoint of the chemical bonding character (19).

Figure 3 shows the temperature dependencies of the magnetic susceptibility for $Ba_3Cr_2MO_9$ (M = Mo and W), where the magnetic susceptibilities are reduced to molar chromium ion. Their magnetic susceptibilities are quite different from each other, although their crystal structures are almost the same. According to the results of structural analysis, magnetic susceptibilities of these $6H$ compounds are considered to obey the dimer-like model (21, 22) or the two-sublattice model (11, 23, 24). In these specimens, if the mean valence of chromium ions is trivalent (i.e., the mean valence of molybdenum or tungsten ion is hexavalent), there is no effective and localized spin moment on molybdenum or tungsten ion; therefore the dimer model for the Cr^{3+}–Cr^{3+} dimer in the face-shared Cr_2O_9 cluster may be applied. The Hamiltonian of the magnetic interaction of the dimer ions i, j bearing electron spins $\mathbf{S}_i$, $\mathbf{S}_j$ is written

$$\mathbf{H} = -2J \sum_{\text{dimer}}^{N} \mathbf{S}_i \cdot \mathbf{S}_j, \qquad [2]$$

where J is the exchange integral in the dimer and is the N number of dimers. Thus, the temperature dependence of the molar magnetic susceptibility for the Cr^{3+}–Cr^{3+} dimer may be represented (21, 22) as

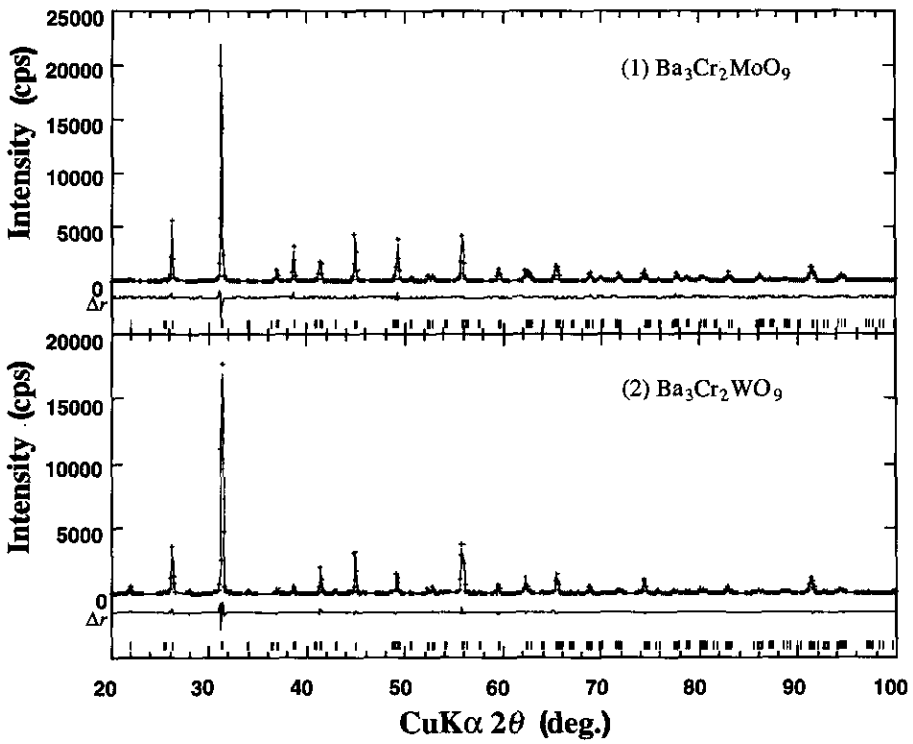

FIG. 1. Observed (solid line) and calculated (crosses) X-ray powder diffraction profiles of $Ba_3Cr_2MoO_9$ and $Ba_3Cr_2WO_9$. Δr indicates the difference between the observed and calculated data. Reflection positions are marked.

$$\chi = \frac{N_A \mu_B^2 \bar{g}^2}{3k_B T}\left[\frac{42 + 15e^{6x} + 3e^{10x}}{7 + 5e^{6x} + 3e^{10x} + e^{12x}}\right], \qquad [3]$$

$$\chi = \frac{N_A \mu_B^2 \bar{g}^2}{3k_B T}\left[\frac{42 + 15e^{6x} + 3e^{10x}}{7 + 5e^{6x} + 3e^{10x} + e^{12x}}\right] + \frac{C}{T - \Theta} + \chi_0, \qquad [4]$$

where $x = -J/k_B T$. Here, N_A, μ_B, and k_B are Avogadro's number, the Bohr magneton, and the Boltzmann constant, respectively. When the specimen includes a small amount of defect or magnetic impurity, the Curie–Weiss term is added to the equation as the second term; then where C, Θ, and χ_0 are the Curie constant, the Weiss temperature, and the temperature independent susceptibility, respectively. The magnetic susceptibility for $Ba_3Cr_2WO_9$ is consistent with this model. The solid line for the raw data in Fig. 3a represents the results fitted to

TABLE 1
Atomic Coordinates and R Factors of $Ba_3Cr_2MoO_9$[a]

Atom	Site	g	x	y	z	B_{eq} (nm^2)
Ba (1)	2*b*	1.0	0	0	1/4	0.004(1)
Ba (2)	4*f*	1.0	1/3	2/3	0.0990(2)	0.006(1)
Cr	4*f*	1.0	1/3	2/3	0.8402(5)	0.004(1)
Mo	2*a*	1.0	0	0	0	0.004(1)
O (1)	6*h*	1.0	0.509(4)	2*x*	1/4	0.000(3)
O (2)	12*k*	1.0	0.1537(35)	2*x*	0.9190(9)	0.000(3)

[a] R_{wp} = 13.33%, R_p = 10.25%, R_r = 11.86%, R_e = 6.31%, R_i = 2.72%, R_f = 1.53%. d = 6.4 g·cm^{-3}; a = 0.56938(2) nm, c = 1.3945(2) nm, space group; $P6_3/mmc$ (No. 194).

TABLE 2
Atomic Coordinates and R Factors of $Ba_3Cr_2WO_9$[a]

Atom	Site	g	x	y	z	B_{eq} (nm^2)
Ba (1)	2*b*	1.0	0	0	1/4	0.003(1)
Ba (2)	4*f*	1.0	1/3	2/3	0.10020(3)	0.007(1)
Cr	4*f*	1.0	1/3	2/3	0.8383(7)	0.004(3)
W	2*a*	1.0	0	0	0	0.003(1)
O (1)	6*h*	1.0	0.49(2)	0.013(9)	1/4	0.000(5)
O (2)	12*i*	1.0	0.17(1)	0.316(6)	0.921(1)	0.000(5)

[a] R_{wp} = 13.51%, R_p = 9.48%, R_r = 10.88%, R_e = 6.97%, R_i = 2.18%, R_f = 1.47%. d = 7.1 g·cm^{-3}; a = 0.56963(5) nm, c = 1.3985(1) nm, space group; $P\bar{6}2c$ (No. 190).

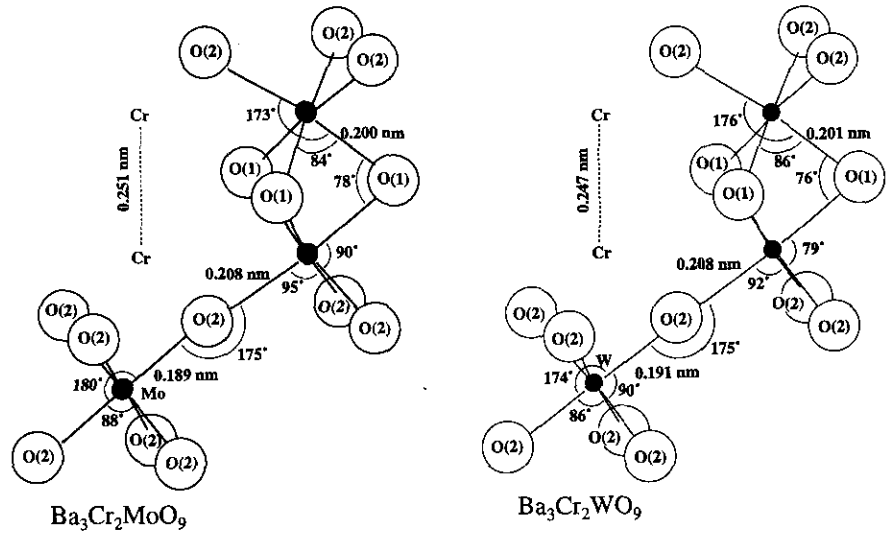

FIG. 2. The *B*-site cation environment of $Ba_3Cr_2MoO_9$ and $Ba_3Cr_2WO_9$.

Eq. [4] with the least-squares method and is calculated from the parameters $\bar{g} = 1.80$, $J/k_B = -161$ K, $C = 0.047$ emu · K · mole^{-1}, $\Theta = -4.9$ K, and $\chi_0 = 1.9 \times 10^{-6}$ emu · K · mole^{-1}. The very small χ_0 value, which may contain the Van Vleck susceptibility (13), does not affect the total susceptibility. The broken line in Fig. 3 represents the C.W. (Curie–Weiss) term in Eq. [4]. When the values of the second and third terms are subtracted from the raw data the residue is well fitted by the dimer term of Eq. [3]. When the C.W. term is attributed to the phase containing solely Cr^{3+} ions, in which Cr^{3+} ions are isolated from each other, we obtain the amount 2.5 mole% of Cr^{3+} as a magnetic second phase using the spin-only value. This ineligible value cannot be attributed to the residual impurity $BaWO_4$ because the W^{6+} ion in this compound is considered to be nonmagnetic. Therefore, the C.W. term is attributed to the Cr^{3+} ion in $Ba_3Cr_2WO_9$. Since the θ value is small, it is plausible to attribute the C.W. term to the Cr^{3+} ions in magnetically isolated octahedra. Such a case can be realized by taking into account the partial disorder in B_1 and B_2 sites. The possibility of partial disorder has also been suggested for $Ba_3Ru_2MgO_9$ (13). The value of J shows an antiferromagnetic interaction and the same order as that of $Ba_3Ru_2MO_9$ (M = Mg, Ca, Sr, and Cd), which contain Ru^{5+} ions with a similar electronic configuration $4d^3(t_{2g}^3)$; e.g., the values of J/k_B for $Ba_3Ru_2MO_9$ are -170 K for M = Ca (13), -173 K for M = Mg (13), -173 K for M = Cd (13), and -138 K for M = Sr (13), respectively. It is well known that the $\bar{g}$ value is given by the spin–orbital coupling constant λ, ligand field gap Δ, and characteristic factor of the covalency of the Cr^{3+}–O^{2-} bond k (13). The smaller $\bar{g}$ value for $Ba_3Cr_2WO_9$ may imply that the Cr^{3+}–O^{2-} bond is fairly ionic due to the strong covalent bond

TABLE 3
Interatomic Distances (nm) and Bond Angles in $Ba_3Cr_2MoO_9$ and $Ba_3Cr_2WO_9$ at Room Temperature

	$Ba_3Cr_2MoO_9$		$Ba_3Cr_2WO_9$	
	Interatomic distances (nm)			
Cr–O (1)	0.200(3)	×6	0.201(3)	×6
Cr–O (2)	0.208(3)	×6	0.208(3)	×6
M–O(2)	0.189(3)	×6	0.191(3)	×6
Ba (1)–O (1)	0.2847(1)	×6	0.28(1) 0.29(1)	×3 ×3
Ba (1)–O (2)	0.280(2)	×6	0.286(2)	×6
Ba (2)–O (1)	0.272(2)	×3	0.270(3)	×3
Ba (2)–O (2)	0.286(2) 0.307(2)	×6 ×3	0.277(7) 0.296(7) 0.304(2)	×3 ×3 ×3
Cr–Cr	0.251(1)	×1	0.247(2)	×1
	Bond angle (degrees)			
Cr–O (2)–*M*	175(1)		175(4)	
Cr–O (1)–Cr	78(1)		76(2)	
O (1)–Cr–O (1)	84(1)		86(1)	
O (1)–Cr–O (2)	173(1) 90(1)		176(1) 91(3) 79(3)	
O (2)–Cr–O (2)	95(1)		92(1)	
O (2)–*M*–O (2)	180 88(1)		174(4) 90(1) 86(3)	

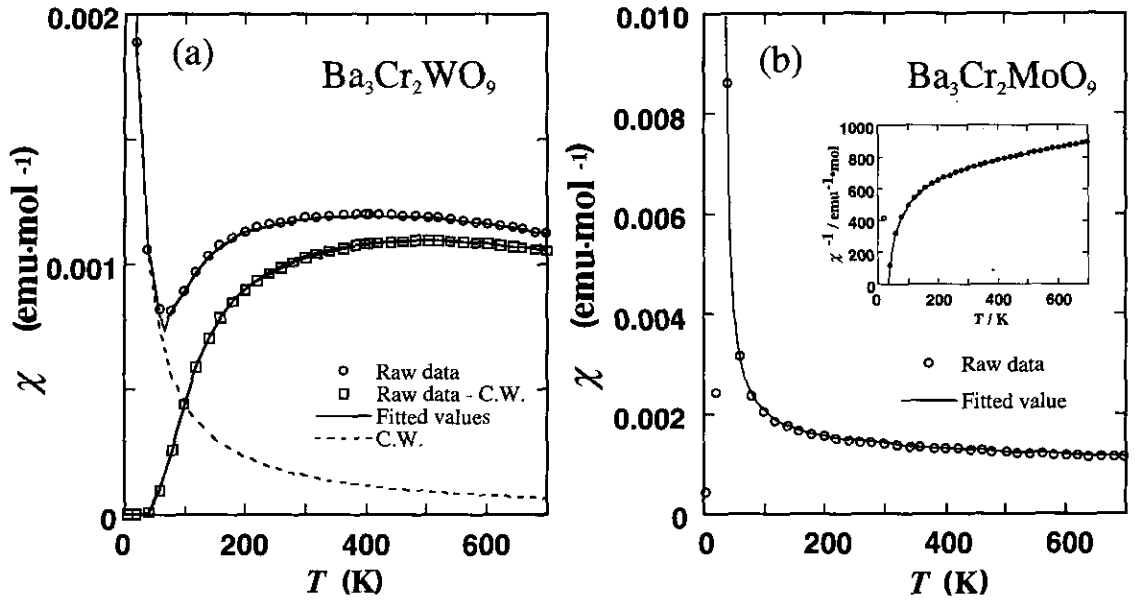

FIG. 3. Temperature dependencies of the magnetic susceptibility for $Ba_3Cr_2MoO_9$ and $Ba_3Cr_2WO_9$. The open circles in (a) and (b) and open squares in (a) show the raw data and contributions of the dimer interaction terms, respectively. The solid lines indicate calculated values from the dimer model and the two-sublattice model. The broken line in (a) shows the contribution of the Curie–Weiss and temperature-independent terms determined by the least squares fitting.

W^{6+}–O^{2-} in the adjacent octahedra. It is to be noted that almost the same value of $J/k_B \approx -170$ K is obtained in the compounds $Ba_3Ru_2MO_9$ and $Ba_3Cr_2WO_9$ in which Ru^{5+} and Cr^{3+} ions have the electronic configurations of $4d^3(t_{2g}^3)$ and $3d^3(t_{2g}^3)$, respectively. This means that the exchange integral J mainly depends on the crystal structure and the electronic configuration of the outermost shell.

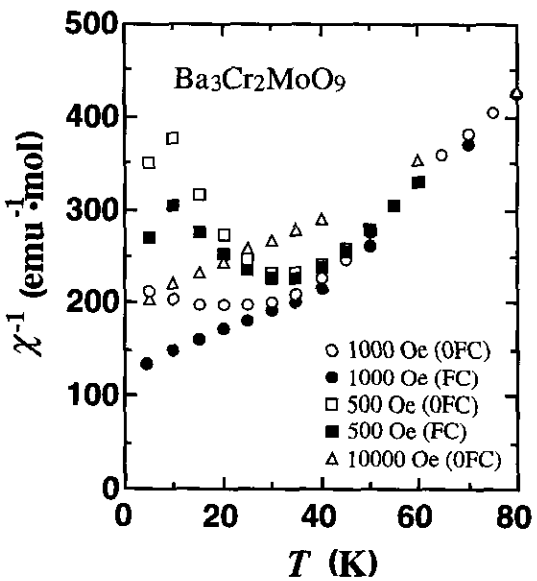

FIG. 4. Temperature dependence of the reciprocal magnetic susceptibility for $Ba_3Cr_2MoO_9$ with various conditions of magnetic field. Open and closed symbols indicate zero-field cooling (0FC) and field cooling (FC), respectively.

If the mean valence of chromium ions is significantly larger than trivalent, an effective and localized spin moment appears on molybdenum and tungsten ions. At this time, two competing interactions coexist, e.g., the ferromagnetic 90° superexchange interaction between Cr ions in the B_2 site and antiferromagnetic 180° superexchange interaction between chromium and molybdenum or tungsten in the B_1 site. In such a case, the two-sublattice model is applied. Goodenough (23) shows the temperature dependence of the magnetic susceptibility in the two-sublattice model, Néel's law, as

$$\chi^{-1} = C^{-1}\left[T - \theta_a - \frac{\theta_b^2}{T-\theta}\right], \qquad [5]$$

where C is a summation of the Curie constants of two sublattices and θ_a, θ_b, and θ, are concerned with the Weiss field inter- and intra-sublattice. In the case of $Ba_3Cr_2MoO_9$, the magnetism obeys the two-sublattice model. In Fig. 3, the thick solid line represents the results fitted by Eq. [5] with the least-squares method in the temperature range from 100 to 700 K and is calculated from the parameters $C = 3.35$ emu·K mole^{-1}, $\theta = -3.52$ K, $\theta_a = -2430$ K, and $\theta_b = 301$ K. The temperature dependence of the magnetic susceptibility for $8H$ Ba_2CrTaO_6 (19) is similar to that for $Ba_3Cr_2MoO_9$. However, since the magnetic susceptibility

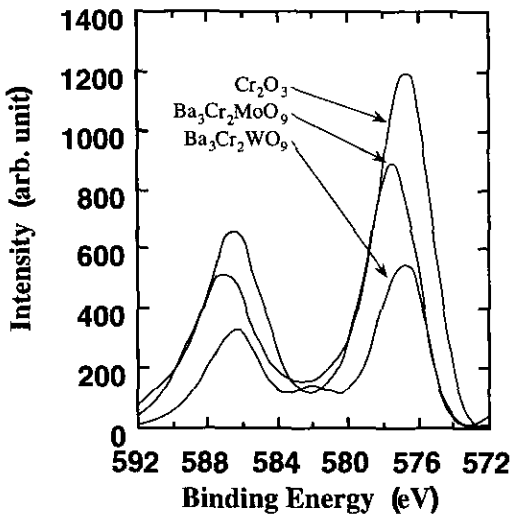

FIG. 5. X-ray photoelectron spectra of Cr $2p$ for Cr_2O_3, $Ba_3Cr_2MoO_9$, and $Ba_3Cr_2WO_9$.

for Ba_2CrTaO_6 could not be explained both by the two-sublattice model and the dimer model, it has been discussed from the viewpoint of covalency between Cr and O or Cr and Cr. Below 70 K, spontaneous magnetization was observed in $Ba_3Cr_2MoO_9$ and the magnetic susceptibility for $Ba_3Cr_2MoO_9$ was found to depend on the measuring conditions, the magnetic field strength, and the cooling conditions under a field or zero-field below 50 K as shown in Fig. 4. This spontaneous magnetization may be attributed to parasitic ferromagnetism or ferrimagnetism. These facts also indicate that the two-sublattice model can be used to explain the magnetism for $Ba_3Cr_2MoO_9$.

Figure 5 shows the X-ray photoelectron spectra of Cr $2p$ for $Ba_3Cr_2MoO_9$, $Ba_3Cr_2WO_9$ and Cr_2O_3. The spectrum of $Ba_3Cr_2WO_9$ is similar to that of Cr_2O_3. Thus, the valence of chromium ion for $Ba_3Cr_2WO_9$ is considered to be +3. On the other hand, the spectrum of $Ba_3Cr_2MoO_9$ is clearly shifted to higher binding energy compared to the others, which means that the valence of chromium ion for $Ba_3Cr_2MoO_9$ is larger than that for $Ba_3Cr_2WO_9$. These results are consistent with the models of the magnetic structure.

CONCLUSION

By the Rietveld analysis for the powder X-ray diffraction data, the crystal structures of the complex oxides, $Ba_3Cr_2MoO_9$ and $Ba_3Cr_2WO_9$ with $6H$ structure, were found to have a similar structure. Chromium ions occupy the center of the face-shared octahedra, while tungsten or molybdenum ions occupy the center of the corner-shared octahedra. The electronic states of molybdenum and tungsten ions were different from each other although they belong to the same 6A group. The magnetic susceptibilities for $Ba_3Cr_2MoO_9$ and $Ba_3Cr_2WO_9$ were explained using the two-sublattice model and the dimer model, respectively. The X-ray photoelectron spectra for Cr support the magnetic models for these compounds.

Clearly more work needs to be done before the magnetic properties of these phases are fully understood.

ACKNOWLEDGMENT

The authors express their thanks for the financial support from the Ministry of Education, Science, and Culture.

REFERENCES

1. J. B. Goodenough and J. M. Longo, *in* "Landolt-Börnstein Numerical Data and Functional Relationships in Science and Technology, New Series, Group 3" (K. H. Hellwege, Ed.), Vol. 4a. Springer–Verlag, New York, 1970.
2. R. W. G. Wyckoff, "Crystal Structures," 2nd ed. Wiley, New York, 1964.
4. R. D. Burbank and H. T. Evans, Jr., *Acta Crystallogr.* **1,** 330 (1948).
3. A. Hardy, *Acta Crystallogr.* **15,** 179 (1962).
5. P. C. Donohue, L. Katz, and R. Ward, *Inorg. Chem.* **4,** 306 (1965).
6. U. Treiber and S. Kemmler-Sack, *J. Solid State Chem.* **43,** 51 (1982).
7. F. Galasso and L. Katz, *Acta Crystallogr.* **14,** 647 (1961).
8. T. Negas, R. S. Roth, H. S. Parker, and W. S. Bower, *J. Solid State Chem.* **8,** 1 (1973).
9. O. Mueller and R. Roy, "The Major Ternary Structural Families." Springer–Verlag, Berlin/New York, 1974.
10. B. M. Collins, A. J. Jacobson, and B. E. F. Fendor, *J. Solid State Chem.* **10,** 29 (1974).
11. K. Kohn, *Solid State Phys.* (in Japanese) **3,** 111 (1968).
12. U. Treiber, S. Kemmler-Sack, and A. Ehamann, *Z. Anorg. Allg. Chem.* **487,** 189 (1982).
13. J. Darriet, M. Drillon, G. Villeneuve, and P. Hagenmuller, *J. Solid State Chem.* **19,** 213 (1976).
14. J. Wilkens and HK. Müller-Buschbaum, *J. Alloys Compounds* **177,** L31 (1991).
15. J. Wilkens and HK. Müller-Buschbaum, *Z. Anorg. Allg. Chem.* **619,** 517 (1993).
16. F. K. Patterson, C. W. Moeller, and R. Ward, *Inorg. Chem.* **2,** 196 (1963).
17. F. Izumi, H. Murata, and N. Watanabe, *J. Appl. Crystallogr.* **20,** 411 (1987).
18. R. D. Shannon, *Acta Crystallogr. Sect. A* **32,** 751 (1976).
19. J.-H. Choy, S.-T. Hong, J.-H. Park, and D.-K. Kim, *Jpn. J. Appl. Phys.* **32,** 4628 (1993).
20. J. B. Goodenough, J. A. Kafalas, and J. M. Longo, *in* "Pressure Methods in Solid State Chemistry." Academic Press, London, 1972.
21. K. Kambe, *J. Phys. Soc. Jpn.* **5,** 48 (1950).
22. F. E. Mabbs and D. J. Nachin, "Magnetism and Transition Metal Complexes." Chapman and Hall, London, 1973.
23. J. B. Goodenough, "Magnetism and the Chemical Bond." Wiley, New York, 1963.
24. R. Aléonard, *J. Phys. Chem. Solids* **15,** 167 (1960).